Compilation of author responses

*We thank you for your careful review and constructive feedback on the manuscript. Below we present responses (in regular font italics) to your comments (**in bold**).*

Minor suggestions:

1. Line 24: Delete "remote sensing".

Thank you. We agree, we have done this.

2. Line 69: "water itself" please note that bbw is different between fresh water and seawater, so need to clarify this statement here.

Thank you for this point. We have edited the sentence to clarify this.

3. Line 74: "Torrecilla and others", I think it should be Torrecilla et al.

We thank the reviewer for this comment. This has been changed to Torrecilla et al., 2011 to follow the style guidelines.

4. Lines 94-111: this summary of current and historical missions is not relevant to this manuscript, could be simply a few citations or reference. Also note that some of the missions are/were not designed for aquatic environments.

We thank the reviewer for the comment. We agree that some of the missions are not directly geared toward aquatic remote sensing, though note that research scientists and operational data managers are opportunistic in use of available sensor data. For example, a robust set of aquatic remote sensing algorithms and products have been developed using Landsat data, a sensor primarily aimed at land remote sensing. For this reason, we provided details on key potentially useful high spectral resolution sensors for interested readers. We have edited the paragraph to reduce the amount of text and narrow the overview of sensors to those especially suited towards high spectral resolution aquatic remote sensing.

5. Line 126: note that Lin et al (2018) have presented a hyperspectral AOP/IOP dataset for the PACE mission.

Lin, J., Lee, Z., Ondrusek, M., & Liu, X. (2018). Hyperspectral absorption and backscattering coefficients of bulk water retrieved from a combination of remote-sensing reflectance and attenuation coefficient. Optics Express, 26(2), 157-177

We thank you for this information. The references listed were an example and not meant to be completely exhaustive. We have added the provided reference in the introduction as suggested.

6. Line 146: "provided at 1 nm resolution". This could be misleading, as the spectral resolution of many radiometers, including HyperPro is ~10 nm. Suggest to change resolution to interval, as it is a simple interpolation of data from much coarser resolution, so not really measurement at 1 nm resolution. This is especially true for bbp, which were usually measured at 6 or 9 bands.

We thank you for this point. We agree that for some data sets, the providers or we interpolated data to integer nm format. We have thus changed "resolution" to "interval" as advised.

7. Line 257: "the spectral region 380–800 nm with a resolution of 3.3 nm" From the document of Satlantic, the spectral resolution is about 10 nm, also the sampling interval is 3.3 nm.

We thank you for this comment. For clarity, we reworded the sentence as advised listing first the resolution, then the sampling interval.

8. Line 265: "a common spectral resolution every 2 nm". Again, it is necessary to be very careful about "resolution", and I think here it is simply a spectral interval of 2 nm for display, not really measured at 2 nm spectral resolution.

We thank you for this comment. We have changed the sentence as recommended.

9. Lines 326-328: "The above-water remote-sensing reflectance spectra were corrected, following the surface correction algorithm of Gould et al. (2001), using the average absorption at 412 nm and the derived spectral scattering shape (Gould et al., 1999)." Suggest to double check and re-word this approach, as it is not clear how average absorption at 412 nm and derived spectral scattering shape can be used to correct surface reflectance in Rrs measurement.

We have revised and added some additional text to briefly describe the steps followed in the Gould et al. 2001 method.

10. "The in situ dataset has been stored and is provided free of charge at the PANGAEA data archive and publisher for Earth and Environmental Science (https://doi.pangaea.de/10.1594/PANGAEA.902230) as detailed in Section 3" This has been presented earlier, which can be deleted here.

We thank the reviewer for this point. We have removed the redundant sentence (which originally appeared at the end of the 1st paragraph of section 4).

Posted author response to review 2

(published 25 November 2019)

*We thank Anonymous Referee #2 for the review and constructive feedback on the manuscript. Below we present responses (in regular font italics) to Anonymous Referee #2 comments (**in bold**).*

Casey et al. provide a well-documented and clearly organized dataset of IOP/AOP covering a diverse range of oceanic environments. I encourage the publication of this dataset. It will be extremely beneficial as planned satellite missions become a reality.

Comments to the authors:

1. I suggest paying special attention to your use of "resolution" in the manuscript as it can be misinterpreted in many of its meanings.

Thank you for this point. We have thoroughly reviewed the manuscript and paid careful attention to ensure consistent and correct use of the word 'resolution'. We have changed 'resolution' to 'sampling interval' where appropriate, as advised by the other reviewer. We have otherwise clarified sentences where appropriate.

2. For Figure 4, consider rearranging subplots to transition geographically, or perhaps organize by the range on the y-axis as it would aid the user/reader in comparing the various regions. Additionally, including a subplot of the map similar to Figure 3 on this Figure would also help with clarity.

We thank the reviewer for this comment. To improve user readability, we have added labels with the cruise name as well as location to the graphs and supplemented the Figure 4 caption. We have kept the order of the graphs the same to remain consistent with the article text, tables and other figures in the paper. In the caption, we refer readers to the map provided in Figure 3 (matching location with cruise names). We find that adding another map to Figure 4 may be repetitious and detract from space to display the spectral reflectance information.

List of all relevant changes made in the manuscript

a) We made all changes detailed in the responses to the reviewer comments above.

b) We added new hyperspectral mission updates regarding the NASA PACE mission and DESIS mission in Section 1.

Marked-up manuscript (follows)

A global compilation of in situ aquatic high spectral resolution inherent and apparent optical property data for remote sensing applications

Kimberly A. Casey[1,2], Cecile S. Rousseaux[1,3,4], Watson W. Gregg[1,3] Emmanuel Boss[5],
Alison P. Chase[5], Susanne E. Craig[4,6], Colleen B. Mouw[7], Rick A. Reynolds[8], Dariusz Stramski[8], Steven G. Ackleson[9], Annick Bricaud[10], Blake Schaeffer[11], Marlon R. Lewis[12], Stéphane Maritorena[13]

[1]Earth Sciences Division, NASA Goddard Space Flight Center, Greenbelt, MD, 20771, USA
[2]Land Resources, U.S. Geological Survey, Reston, VA, 20192, USA
[3]Global Modeling and Assimilation Office, NASA Goddard Space Flight Center, Greenbelt, MD, 20771, USA
[4]Universities Space Research Association, Columbia, MD, 20771, USA
[5]School of Marine Sciences, University of Maine, Orono, ME, 04469, USA
[6]Ocean Ecology Laboratory, NASA Goddard Space Flight Center, Greenbelt, MD 20771, USA
[7]University of Rhode Island, Graduate School of Oceanography, Narragansett, RI, 02882, USA
[8]Marine Physical Laboratory, Scripps Institution of Oceanography, University of California San Diego, La Jolla, CA, 92093, USA
[9]Naval Research Laboratory, Washington, D.C., USA, 20375
[10]CNRS and Sorbonne Université, Laboratoire d'Océanographie de Villefranche (LOV), F-06230 Villefranche-sur-mer, France
[11]Office of Research and Development, U.S. Environmental Protection Agency, USA
[12]Department of Oceanography, Dalhousie University, Halifax, Nova Scotia, Canada
[13]Earth Research Institute, University of California, Santa Barbara, CA, 93106, USA

Correspondence to: Kimberly A. Casey (kimberly.a.casey@nasa.gov, kcasey@usgs.gov)

Deleted: Kimberly.A.Casey

Deleted: remote sensing

Abstract. Light emerging from natural water bodies and measured by radiometers contains information about the local type and concentrations of phytoplankton, non-algal particles and colored dissolved organic matter in the underlying waters. An increase in spectral resolution in forthcoming satellite and airborne remote sensing missions is expected to lead to new or improved capabilities to characterize aquatic ecosystems. Such upcoming missions include NASA's Plankton, Aerosol, Cloud, ocean Ecosystem (PACE) Mission; the NASA Surface Biology and Geology observable mission; and NASA Airborne Visible / Infrared Imaging Spectrometer - Next Generation (AVIRIS-NG) airborne missions. In anticipation of these missions, we present an organized dataset of geographically diverse, quality-controlled, high spectral resolution inherent and apparent optical property (IOP/AOP) aquatic data. The data are intended to be of use to increase our understanding of aquatic optical properties, to develop aquatic remote sensing data product algorithms, and to perform calibration and validation activities for forthcoming aquatic-focused imaging spectrometry missions. The dataset is comprised of contributions from several investigators and investigating teams collected over a range of geographic areas and water types, including inland waters, estuaries and oceans. Specific in situ measurements include coefficients describing particulate absorption, particulate attenuation, non-algal particulate absorption, colored dissolved organic matter absorption, phytoplankton absorption, total absorption, total attenuation, particulate backscattering, and total backscattering, as well as remote-sensing

reflectance, and irradiance reflectance. The dataset can be downloaded from https://doi.pangaea.de/10.1594/PANGAEA.902230 (Casey et al., 2019).

1 Introduction

Remote sensing of Earth's aquatic areas is a powerful tool for understanding water quality, aquatic and ecological dynamics, and the concentrations and types of phytoplankton, colored dissolved organic matter and non-algal particles present over time. Aquatic remote sensing initially focused on chlorophyll-a concentration ([Chl]) (NASA GSFC, Ocean Biology Processing Group, 2014) which serves as a proxy for understanding the distribution of phytoplankton biomass. The most widely used approach to estimate [Chl] has been empirical relationships between band ratios or band differences of remotely sensed reflectance and [Chl] (O'Reilly et al. 1998; Hu et al. 2012). Chlorophyll-a concentration estimated from aquatic color has been studied for many decades and remote sensing retrievals are well validated (McClain, 2009). Chlorophyll algorithm improvements continue in response to enhanced spectral resolution and sensor capabilities of upcoming Earth Observation missions (O'Reilly and Werdell, 2019). Aquatic remote sensing is now being further used to aid the understanding of more complex dynamics including atmosphere–ocean heat exchange and the role and feedback effects of aquatic constituents, as well as alteration of phytoplankton community structure in a changing climate (Kim et al., 2018; Dutkiewicz et al., 2019; Del Castillo et al., 2019). These analysis approaches involve numerical modeling and analyzing radiometric variability of many spectral bands.

In situ data is a key requirement for aquatic remote sensing algorithm development, validation and calibration activities and for advancing our aquatic remote sensing data capabilities. The in situ data provided in this manuscript include inherent optical properties (IOPs) and apparent optical properties (AOPs) from a wide distribution of aquatic environments and geographic locations. Briefly, inherent optical properties are the light absorption and scattering properties of the natural waters which are dependent solely on the concentrations and composition of water constituents irrespective of the illumination field within a water body. An apparent optical property is an optical property that can be used as a descriptor of a water body and is primarily dependent on the IOPs of the aquatic medium and, to a lesser degree, on the directional structure of the ambient radiance distribution within a water body. In this article, we provide data for the AOPs of irradiance reflectance (R) and radiance-reflectance or remote-sensing reflectance (R_{rs}) just above the water surface, and for the IOPs representing absorption and backscattering coefficients of natural waters. The spectral IOPs (where λ is light wavelength in a vacuum) can be partitioned into the absorption due to water ($a_w(\lambda)$, m^{-1}), phytoplankton ($a_{ph}(\lambda)$, m^{-1}), non-algal particles ($a_{nap}(\lambda)$, m^{-1}), colored dissolved organic matter ($a_{cdom}(\lambda)$, m^{-1}), and backscattering due to water ($b_{bw}(\lambda)$, m^{-1}) and particles ($b_{bp}(\lambda)$, m^{-1}), where we note that b_{bw} differs according to the salinity of the water.

With coincident high spectral resolution in situ IOP and AOP data, scientists can better develop and validate aquatic remote sensing algorithms to derive IOPs from measured AOPs (e.g. Werdell et al., 2018, and references therein). Torrecilla et al., 2011, demonstrated that hyperspectral data of phytoplankton absorption and remote-sensing

2

reflectance provide improved discrimination of dominant phytoplankton groups in open-ocean environments compared with multi-spectral data. High spectral resolution aquatic remote sensing significantly improves retrievals of optical constituents in inland, coastal and polar aquatic environments, where these environments exhibit significant smaller-scale temporal and spatial variability, increased decoupling between in-water constituents, and a greater dynamic range in parameter values compared to the open ocean (Mouw et al., 2015; Bell et al., 2015; Dierssen et al., 2015; Hu et al., 2015; Vandermeulen et al., 2017). In inland, coastal and polar aquatic areas, dissolved organic matter (DOM) and non-algal particles (NAP) play a more important role in affecting the color of water as well as its biogeochemistry, sediment transport, and primary productivity (Devred et al., 2013; Mouw et al., 2017). Thus, greater measurement precision is desirable. Carbon pools are also varied in inland and coastal environments due to riverine inputs, terrestrial influence, resuspension and mixing requiring greater spectral resolution and broader spectral range to differentiate the spectral slope of CDOM sources. Further, there are increased instances of harmful algal bloom formation in many aquatic environments. Some harmful algal blooms can be discriminated based on their unique optical signatures and therefore additional spectral bands beyond the current multi-spectral capabilities would be highly beneficial (Wang et al. 2016, Pahlevan et al., 2019). Moving geographically to polar latitudes, Neukermans and others (2016) demonstrated improved discrimination of planktonic communities in the Arctic by using hyperspectral instead of multispectral satellite data. In short, remote sensing capabilities in all aquatic environments are expected to improve considerably in precision and accuracy with high radiometric quality high spectral resolution measurements.

We summarize many of the historic, current and forthcoming high spectral resolution missions of greatest applicability to aquatic remote sensing goals in Figs. 1 and 2. High spectral resolution technological demonstration satellite missions that have flown or are currently in operation or late planning stages are detailed as follows. One of the longest spaceborne hyperspectral data records is provided by NASA's EO-1 Hyperion sensor (220 spectral bands from 400 to 2500 nm), which was launched on 21 November 2000 and decommissioned on 22 February 2017. Another long high spectral resolution temporal record (2001 to present) is provided by the European Space Agency's Compact High Resolution Imaging Spectrometer (CHRIS), able to acquire up to 63 spectral bands from 400–1050 nm. The Naval Research Laboratory had the first water focused hyperspectral sensor, the Hyperspectral Imager for the Coastal Ocean (HICO) on the International Space Station (ISS) with more than 80 bands and providing 5 years of data (September 2009–2014) (Corson and Davis, 2011). The DLR Earth Sensing Imaging Spectrometer (DESIS), which contains 235 spectral bands from 400-1000 nm, was installed on the ISS in August 2018 and is expected to operate several years (Krutz et al., 2019). The Italian Space Agency launched the Hyperspectral Precursor of the Application Mission (PRISMA) mission in March 2019. Germany plans to launch the Environmental Mapping and Analysis Program (EnMAP) upon completion of Phase D, notionally in 2020. Ongoing airborne missions of high spectral resolution capabilities include instruments such as NASA's Airborne Visible-Infrared Imaging Spectrometer-Next Generation (AVIRIS-NG) and an airborne hyperspectral sensor, HyMap. Many other high spectral resolution satellite and airborne missions are in recent operation or deployment stages, such details can be gleaned for example from the Committee on Earth Observation Satellites (CEOS) database (http://database.eohandbook.com).

Deleted: satellite

Deleted: potentially applicable

Deleted: ,

Deleted: Hyperion had 220 spectral bands from 400 to 2500 nm, providing continuous, 10 nm spectral resolution.

Deleted: CHRIS was launched aboard Proba-1 on 22 October 2001 and is operational at present.

3

125

NASA's Plankton, Aerosol, Cloud, ocean Ecosystem (PACE) satellite mission is intended to be a hyperspectral atmospheric and ocean color mission to be launched in 2022–2023 and to provide data to further the understanding of a myriad of Earth system processes including those involving ocean ecology, biogeochemistry, as well as atmospheric composition and dynamics (see more details in Werdell et al., 2019). One of the central objectives of the PACE

130 mission is to improve our understanding and quantification of the aquatic biogeochemical cycling and ecosystem function in response to anthropogenic and natural environment variability and change. High spectral resolution coincident IOP/AOP data are required to aid in development and refinement of algorithms to characterize and quantify aquatic conditions and for the calibration and validation of satellite measurements. The Surface Biology and Geology mission is an additional likely upcoming U.S. space agency hyperspectral mission. It has been recommended as the

135 first Earth Observation mission to come following the currently scheduled remote sensing missions. This Surface Biology and Geology mission is targeted to collect hyperspectral visible–shortwave infrared imagery and multi- or hyperspectral thermal imagery, at 30–60 m spatial resolution and will include measurements of inland and coastal environments (National Academies of Sciences, Engineering, and Medicine, 2018).

140 At present, there is a paucity of coincident in situ optical aquatic measurements of high spectral resolution. There are databases providing multispectral resolution IOPs and AOPs, with varying degrees of updates in recent years (e.g. Werdell and Bailey, 2002; Werdell and Bailey, 2005; Lin et al, 2018; Valente et al., 2019). We present the first organization of existing quality-controlled hyperspectral IOP and AOP data from polar, open ocean, estuary, coastal, and inland water. The dataset is intended for remote sensing algorithm development activities associated with

145 upcoming high spectral resolution satellite and airborne missions.

2 Materials and Methods

In 2015, in the early development of the PACE Mission, there was an open call to the aquatic remote sensing community to contribute well-documented, quality-controlled data sets consisting of near-synchronous depth profiles

150 of IOPs and AOPs within the water column and near-surface reflectance and optical properties as part of an international effort to build a dataset for algorithm development and testing. All contributors to the database have actively taken part in the quality assessment of the data. Variable assignments, accuracy estimates, and measurement details were given and confirmed by the data providers. Data that either had IOP or AOP at high spectral resolution were included in the dataset. To arrange data in an organized, uniform structure, data were edited as follows. Data

155 were filtered by considering depths from the surface to no greater than 50 m depth. We rounded data provided at fractional wavelengths to the nearest integer. Missing data is represented in the data files by placeholder values of −999. Metadata is provided at the top of each data file, detailing the contact information for the data provider, the file source, data publication reference(s), native data collection range and resolution. The spectral range of the database is 300–900 nm, provided at a 1 nm interval. Variables included in the database are listed in Table 1. Data collection

160 characteristics are presented in Table 2. Figure 3 and Table 3 detail the global distribution of coincident IOP/AOP

4

data. In general terms, AOPs were measured using commercially available radiometer systems that either float at the surface or vertically profile the water column. IOPs were measured using in-water instrumentation and
165 spectrophotometric analysis of discrete water samples (i.e. water sample removed from the aquatic environment). Brief descriptions of provider and cruise-specific protocols and methodology are given in the following paragraphs.

2.1 Methods by Data Contributor and Expedition

In this section, the data providers describe their specific data collection methods used in acquiring and processing the
170 provided data. Methods not previously published in peer reviewed literature are detailed fully here.

2.1.1 Ackleson – RIO-SFE-1 and RIO-SFE-3

Ackleson provides in situ data from the Remote and In Situ Observations - San Francisco Bay and Delta Ecosystem (RIO-SFE) data collection efforts over nine stations in the bay area of San Francisco, California, USA. In-water
175 spectral absorption and attenuation were measured using a WETLabs AC-S and AC-9. The AC-9 intake was passed through a 0.7 μm cartridge filter to remove particulates, thus, those measurements represent only very small particles and dissolved impurities (a_{cdom} and c_{cdom}). The particulate absorption coefficient, $a_p(\lambda)$, was calculated from the difference between AC-S measurements of whole water, $a(\lambda)$ and ac-9 $a_{cdom}(\lambda)$. Backscattering, $b_b(\lambda)$, was measured by a WETLabs ECO-VSF 3.
180

Above-water $R_{rs}(\lambda)$ was measured between 400 nm and 900 nm using an Analytical Spectral Devices (ASD; Boulder, CO) handheld Spectrometer. The procedure for measuring reflectance is a modified version of Carder and Steward (1985). At each station, 10 sets of measurements were made consisting of 1) reflected radiance from a Spectralon 10% reflectance plaque (Labsphere, Inc., North Sutton, NH), 2) radiance reflected from the sea surface, and 3) radiance
185 from the section of the sky that would be reflected off the sea surface at the measurement angle. These repetitions were completed as rapidly as possible in order to minimize the impact of changing light or water conditions. Measurements were made between 90° and 135° azimuthal angle relative to the position of the sun and at a 30° angle relative to the vertical to minimize sun glint (Mobley and Stramski, 1997; Mobley 1999).

190 **2.1.2 Boss, Chase – Tara Expeditions and SABOR**

The Tara Oceans expedition was a two-and-a-half-year long ocean cruise, intended to provide a sampling of the world's diverse ocean environments. The Tara Oceans Polar Circle Expedition (Tara Arctic) took place from May through December 2013 and allowed collection of data in the Arctic Ocean. The Tara Mediterranean expedition (Tara Med) took place from June through September 2014 in the Mediterranean Sea. The Ship-Aircraft Bio-Optical
195 Research (SABOR) collaborative research campaign allowed scientists to gather data from the Gulf of Maine, North Atlantic and Mid-Atlantic coast from July thru August 2014. A full description of these Tara and SABOR expeditions

and the Boss/Chase provided IOP and AOP datasets and data processing can be found in Boss et al., 2013, Chase et al., 2017, and Matsuoka et al., 2017. Briefly, IOPs were measured by an inline system that included a WET-Labs AC-S, a CDOM fluorometer and a thermosalinograph. Particulate properties were computed from the difference between measurements of the total and dissolved fraction (Dall'Olmo et al., 2009; Slade et al., 2010). Absorption by the dissolved fraction was computed by interpolating between daily discrete samples collected with a 2 m long Ultra Path capillary wave guide using the filtered AC-S measurements (Matsuoka et al., 2017). During the Tara Oceans/Mediterranean and the SABOR campaigns, reflectance was measured using a Satlantic hyper-spectral radiometer buoy (a.k.a. HyperPro in buoy mode), with radiance measured by the upwelling radiometer and propagated to the surface using a bio-optical model, and then used together with downwelling irradiance to calculate remote-sensing reflectance ($R_{rs}(\lambda)$) (see Chase et al., 2017 for details on data processing). During the Tara Arctic campaign, a C-OPS profiling radiometer system was used to measure upwelling radiance and downwelling irradiance and subsequently calculate $R_{rs}(\lambda)$ at 19 wavelengths between 320 nm and 880 nm.

2.1.3 Bricaud – BIOSOPE

The BIogeochemistry & Optics SOuth Pacific Experiment (BIOSOPE) cruise on R/V l'Atalante, from October through December 2004 followed an 8000 km transect from the mesotrophic waters around the Marquesas Islands to the hyperoligotrophic waters of the South Pacific Gyre, and then to the eutrophic waters of the upwelling area off Chile. BIOSOPE was a collaborative cruise where participating investigators were responsible for making subsets of optical measurements. With the combined data of the contributing BIOSOPE investigators, nearly all BIOSOPE campaign stations contain complete sets of AOP and IOP data. This section summarizes Bricaud's methodologies in BIOSOPE campaign data collection. A detailed description of the dataset and methods can be found in Bricaud et al. (2010).

Particulate and CDOM absorption measurements were made on board. For particulate absorption measurements, seawater samples were collected on Whatman GF/F filters, and absorption spectra, $a_p(\lambda)$, were measured using the filter pad technique (with a soaked blank filter as a reference), using a Perkin-Elmer Lambda-19 spectrophotometer equipped with an integrating sphere. Non-algal absorption spectra, $a_{nap}(\lambda)$, were measured on the same filters after pigment extraction in methanol (Kishino et al. 1985). When necessary, the residual absorption due to incompletely extracted pigments was corrected by applying an exponential fit (over the wavelength ranges where pigment absorption is negligible) to actual spectra.

All spectra were shifted to zero in the near infrared (750–800 nm average) to minimize possible differences between sample and reference filters. Measured optical densities were corrected for the pathlength amplification effect (according to Allali et al. 1997 for clear waters, and to Bricaud and Stramski, 1990 for eutrophic waters) and then converted into absorption coefficients (in m^{-1}). Finally, phytoplankton absorption spectra, $a_{ph}(\lambda)$, were obtained by subtracting $a_{nap}(\lambda)$ from $a_p(\lambda)$.

6

CDOM absorption measurements were performed using a WPI Ultrapath capillary waveguide with a 2 m pathlength. Samples were filtered under dim light into glass bottles, using pre-rinsed 0.2 μm Sartorius filters, and then analysed immediately. High-performance liquid chromatography quality water, artificially salted (35 g L^{-1}) with precombusted NaCl, was used as reference water. Between each measurement, the sample cell was cleaned according to the WPI, Inc. recommendations. Replicate measurements (including all handling steps) showed that the reproducibility was approximately $\pm$ 0.005 m^{-1} at 375 nm.

2.1.4 Craig – BBOMB

All measurements from provider Craig are derived from collection of data at the Bedford Basin Ocean Monitoring Buoy (BBOMB), a coastal ocean monitoring buoy located in the Bedford Basin near Halifax, Nova Scotia, Canada. A full description of the Craig dataset and acquisition protocols can be found in Craig et al. (2012). Water samples were collected by Niskin bottle at a depth of 1 m for the determination of various water column parameters, that included spectral particulate absorption coefficient, $a_p(\lambda)$ and $a_{cdom}(\lambda)$. Wherever possible, NASA Ocean Optics Protocols (Pegau et al., 2003) were followed for all sample acquisition, handling, storage and analysis. Briefly, $a_p(\lambda)$ and $a_{ph}(\lambda)$ spectra were determined from water samples that were filtered under low pressure through a 25 mm GF/F (Whatman) filter. The particulate absorption coefficient, $a_p(\lambda)$, in the range 350–800 nm was determined in a Cary UV–VIS spectrophotometer with the filter pad mounted on a quartz glass slide and placed at the entrance to an integrating sphere in a modification (Craig, 1999) of the Shibata (1959) opal glass technique. Samples were de-pigmented by soaking the filters in a 0.1% active chlorine solution of NaClO (Kishino et al., 1985; Tassan and Ferrari, 1995). The absorption spectra of the de-pigmented particles, $a_{nap}(\lambda)$, were then measured as described above and $a_{ph}(\lambda)$ calculated from $a_p(\lambda) - a_{nap}(\lambda)$.

Depth profiles of hyperspectral downwelling irradiance, $E_d(\lambda, z)$ (μW cm^{-2} nm^{-1}) and upwelling radiance, $L_u(\lambda, z)$ (μW cm^{-2} nm^{-1} sr^{-1}) (where z is depth in the water column) were made with a HyperPro (Satlantic Inc.) profiling radiometer. Multiple casts (usually three) were made in quick succession and ~100 m away from the boat to avoid the influence of ship shadow (Mueller et al., 2003). A deck unit mounted to the superstructure of the boat also provided contemporaneous measurements of above-water surface incident irradiance, $E_s(\lambda)$, during profile acquisition.

2.1.5 Lewis – BIOSOPE

Another participating science investigator on the BIOSOPE campaign was M. Lewis. This section details his collection of BIOSOPE cruise data. Remote sensing spectral reflectance ($R_{rs}(\lambda)$, sr^{-1}, specifically, the ratio of water-leaving radiance to downwelling irradiance above sea surface) in the South Pacific gyre was computed from direct measurements of downwelling irradiance above the sea surface ($E_s(\lambda)$, W m^{-2} nm^{-1}) taken aboard ship, and measurements of upwelling radiance ($L_u(\lambda)$, W m^{-2} nm^{-1} sr^{-1}) made at a depth of 20 cm below the ocean surface, using

a modified hyperspectral profiling radiometer adapted to float at the sea-surface and tethered such that the instrument operated at a distance of ~100 m from the vessel (HyperPro, Satlantic; Claustre et al., 2008; Stramski et al., 2008; Lee et al., 2010). Instrument tilt was measured directly; measurements were rejected if tilts exceeded 5 degrees. Measurements were made over the spectral region 380–800 nm via an instrument resolution of 10 nm and a sampling interval of 3.3 nm. Dark values were taken every five samples by use of an internal shutter. These were linearly interpolated for each light value, and then subtracted from the observations. Calibration coefficients and corrections for immersion effects were obtained following standard protocols (Mueller et al., 2003) and applied to the measurements; demonstrated absolute accuracies are < 2.8% for radiance and < 2.1% for irradiance (see Gordon et al., 2009). Irradiance and radiance data were taken for 3 minutes at each deployment, with each observation within the deployment time-series representing integration times of 0.03 to 0.5 seconds, depending on the intensity of the incident radiance. These measurements were then interpolated to a common time frame at a frequency of 2 seconds and 2 nm spectral interval.

Upwelling radiance measurements were then propagated to the sea-surface using an iterative approach that estimates the spectral diffuse attenuation coefficient from spectral ratios of measured radiance, and the water-leaving radiance above the sea surface, $L_W(\lambda)$, is then computed based on Fresnel reflectance at the water–air boundary and the real relative index of refraction of water (Mueller et al., 2003). A 3 minute time series of R_{rs} was made by dividing the computed water-leaving radiance by the downward irradiance for each time interval, and an average value and standard deviation computed for each deployment.

2.1.6 Mouw – Lake Superior Studies

Provider Mouw contributed data from measurements made by researchers at the University of Rhode Island in the inland water body, Lake Superior, the largest of the Great Lakes of North America. A detailed description of the methods used for inland IOP and AOP observations can be found in Mouw et al. (2017). Optical and biogeochemical data were collected in Lake Superior during the ice-free months (May–October) of 2013 through 2016. The dataset consists of a full suite of coincident IOPs and AOPs, including a, a_{cdom}, a_{cdom_dis}, a_{nap_dis}, a_{nw}, a_p, a_{p_dis}, b_b, b_{bp}, c, c_{nw}, and $R_{rs}(\lambda)$. The variables used to retrieve R_{rs} are available by request from the data contributor. The contributor also notes that a_{ph} can be calculated from the provided variables.

AOP radiometric measurements were made with three HyperOCR spectral radiometers (Satlantic Inc.) that measure between 350 nm and 800 nm with an approximately 3 nm sampling interval (137 total wavelengths). In-water $E_d(\lambda)$ and $L_u(\lambda)$ HyperOCR sensors were attached to a free-falling Profiler II frame (Satlantic Inc.), while the $E_s(\lambda)$ sensor was mounted on top of the ship to allow for correction of the other measurements due to changing sky conditions. At each station, the system was deployed for three cast types: surface, multi- and full profile. To characterize the air–water interface, a floatation collar on the profiler frame enabled continuous measurement of $L_u(\lambda)$ approximately 20 cm below the water surface for 5 minutes (surface profile). The flotation collar was removed, and the profiler then

deployed in free-fall mode, measuring five consecutive profiles from the surface to 10 m to characterize the near-surface light field (multi-profile). Finally, the profiler was allowed to free-fall to the 1% light level or to within 10 m of the bottom, whichever was shallower (full profile). All methods and analysis follow the NASA ocean optics protocols for satellite ocean color sensor validation (Mueller et al., 2003).

315

IOPs were collected via a vertically profiled bio-optical package that measures absorption, attenuation (WET Labs AC-S) and backscattering (WET Labs ECO-BB9) along with concurrent temperature, salinity (SeaBird CTD 37SI) and fluorometeric chlorophyll a (WET Labs ECO-FL3). All methods and analysis followed the NASA ocean optics protocols for satellite ocean color sensor validation (Mueller et al., 2003). Total absorption and attenuation ($a(\lambda)$ and

320    $c(\lambda)$, m^{-1}, respectively) were resolved at 81 wavelengths between 400–750 nm.

For laboratory analysis of discrete water samples, spectral CDOM, particulate, non-algal and phytoplankton absorption were measured spectrophotometrically (Perkin-Elmer Lambda 35 UV/VIS dual-beam) for wavelengths between 300 nm and 800 nm. Absorption of CDOM filtrate was measured in a 10 cm cuvette following NASA's

325   Ocean Optics Protocols (Mueller et al., 2003) using a slit-width of 2 nm and a scan rate of 240 nm min^{-1}. For particulate and non-algal absorption, we followed the transmission–reflectance (T−R) method (Tassan and Ferrari, 2002; Lohrenz, 2000; Lohrenz et al., 2003) that utilizes an integrating sphere to correct measurements for the contribution of scattering.

330   **2.1.7 Schaeffer – Florida Estuary Optics**

Provider Schaeffer collected in situ measurements and water samples during boat-based surveys in Florida estuaries between September 2009 and November 2011. Hydrographic profiling measurements were collected using a Seabird CTD package. A free-falling hyperspectral profiling system (HyperPRO, Satlantic, Halifax, NS, Canada) provided in-water hyperspectral (400–735 nm, interpolated every 1 nm) measures of downwelling irradiance ($E_d(z,\lambda)$),

335   upwelling radiance ($L_u(z,\lambda)$), and depth (z). Water samples were collected 0.5 m below the air-water surface for absorption (phytoplankton pigment, non-algal particles, CDOM) and extracted chlorophyll analyses. CDOM absorption was measured in a 10 cm cuvette using a Shimadzu UV1700 dual-beam spectrophotometer at 1 nm intervals between 200–700 nm with Milli-Q deionized water as a reference. Total particulates were collected on Whatman 25 mm GF/F filters and analyzed with a Shimadzu UV1700 dual-beam spectrophotometer at 1 nm intervals between

340   400–800 nm with 0.2 μm filtered seawater as the reference standard (Pegau et al., 2003). Pigments were extracted from filters with warm methanol and rescanned to measure the detrital absorption (Kishino et al., 1985).

Remote-sensing reflectance (R_{rs}) was derived from both a profiling radiometer (HyperPro, Satlantic) and a hyperspectral surface acquisition system (HyperSAS, Satlantic Inc., Halifax, Nova Scotia). The HyperSAS logged

345   spectral measurements of above-water radiance ($L_t(\lambda)$), sky radiance ($L_i(\lambda)$), and downwelling sky irradiance ($E_s(\lambda)$) from 350 to 800 nm (interpolated at 1 nm intervals). The above-water remote-sensing reflectance (R_t) spectra were

9

corrected for reflected sky light, sun light, sun glint, and reflected cloud light, following the second path surface correction algorithm of Gould et al. (2001) to derive the final corrected remote-sensing reflectance (R_{rs}). Specifically, in Gould et al. (2001), $R_{rs}(\lambda) = R_t(\lambda) - (A\,R_{sky}(\lambda) + B)$, where R_{sky} is the corrected sky spectra, A is the sea surface reflectance factor, and B is a residual offset. R_t was coupled with in-water measurements of absorption at 412 nm, scattering at 412 nm, and scattering shape to correct for surface reflection. Florida Estuaries archived data is available at https://doi.org/10.23719/1424031.

2.1.8 Stramski, Reynolds – BIOSOPE, ANT26, KM12

Stramski and Reynolds provide data for three cruises, BIOSOPE, ANT26 and KM12. ANT26 was a German cruise onboard the R/V Polarstern, covering a south-to-north segment of the Atlantic Ocean from Punta Arenas, Chile area (beginning in April 2010) to Bremerhaven, Germany area (finishing in May 2010). The KM12 cruise collected data in the Pacific Ocean off the Hawaiian Islands in June 2012. For all three cruises, the spectral backscattering coefficient of seawater, $b_b(\lambda)$, was measured in situ from vertical profiles obtained with a combination of HOBI Labs Hydroscat-6 and a-βeta sensors. The determination of $b_b(\lambda)$, and the particulate contribution $b_{bp}(\lambda)$ from these measurements is described in Stramski et al. (2008) and Zheng et al. (2014). On BIOSOPE, a Hydroscat-6 providing measurements at six wavelengths (442, 470, 550, 589, 620, and 671 nm) was paired with two single wavelength a-βeta sensors (420 and 510 nm). For the ANT26 and KM12 cruises, a combination of two Hydroscat-6 instruments was used to provide measurements in eleven spectral bands (394, 420, 442, 470, 510, 532, 550, 589, 640, 730, and 852 nm; 550 nm common to both instruments).

For the ANT26 and KM12 cruises, discrete water samples within the upper 5 m were collected from a CTD-Rosette equipped with Niskin bottles. The spectral absorption coefficient of particulate material, $a_p(\lambda)$, was determined spectrophotometrically with a filter pad technique for particles retained on a 25 mm glass fiber filter (GF/F, Whatman). Measurements were made at 1 nm sampling interval over the spectral region 300–850 nm using a Perkin-Elmer Lamba 18 spectrophotometer equipped with a 15 cm diameter integrating sphere. The filters were placed inside the sphere to minimize potential scattering error, and the correction for pathlength amplification factor determined for this configuration of measurement was used (Stramski et al., 2015). The partitioning of $a_p(\lambda)$ into phytoplankton, $a_{ph}(\lambda)$, and non-algal particle, $a_{nap}(\lambda)$, contributions was accomplished through the chemical extraction of pigments using methanol (Kishino et al., 1985). The absorption coefficient of CDOM, $a_{cdom}(\lambda)$, on ANT26 was determined on discrete water samples using a PSICAM instrument (Röttgers and Doerffer, 2007). For KM12, a_{cdom} was measured in situ using a WET Labs AC-S.

The spectral remote-sensing reflectance, $R_{rs}(\lambda)$, for the ANT26 and KM12 cruises was determined by averaging a time-series of radiometric measurements from a Satlantic HyperPro II radiometer attached to a surface float and deployed at a large distance from the vessel. Measurements were obtained over the spectral range 350–800 nm approximately every 3 nm and subsequently interpolated to 1 nm intervals. Subsurface measurements of the upwelling

10

zenith radiance (i.e., light propagating towards zenith) made at 0.2 m depth were propagated to and across the sea-surface and combined with above-surface measurements of downwelling planar irradiance to estimate $R_{rs}(\lambda)$ (Uitz et al., 2015).

3 Data Availability

395 The diverse set of in situ apparent and inherent optical property data are stored and provided free of charge at the PANGAEA data archive and publisher for Earth and Environmental Science. Data are available as Microsoft Excel (.xlsx) files. The primary link for accessing the data is https://doi.pangaea.de/10.1594/PANGAEA.902230 (Casey et al., 2019). Individual variable files are stored and available via interactive HTML download at
400 https://doi.pangaea.de/10.1594/PANGAEA.902230?format=html#download or via tab-delimited text at https://doi.pangaea.de/10.1594/PANGAEA.902230?format=textfile.

4 Results and Discussion

Overall, the collection of datasets provides mostly coincident IOP/AOP data from a wide range of latitudes and water
405 types, including polar, open ocean, estuary, coastal and inland water environments. We detailed the specific cruise, instrument and methodology approaches taken by each data provider. The majority of the data has been published as referenced. The few contributed data sets which are not yet published in peer reviewed literature are fully described in this manuscript. Thus, the data provide a robust means to evaluate aquatic remote sensing observations toward further remote sensing science research and development goals.
410

Hereafter we describe the spatial and temporal resolution covered by the dataset for coincident IOP and AOP, where when referring to coincident data, we describe data that have R_{rs} and at least one IOP variable available. IOP and AOP data are provided from 12 cruises, from 2004 through 2016, covering Arctic, mid- and equatorial open ocean, estuary, coastal and inland aquatic sites (see Table 2, Fig. 3). A summary of the number of data points available for every
415 cruise for each of the variables is provided in Table 3. Table 3 shows that IOPs are generally collected at more stations than AOPs. The number of data available for IOPs is also much larger than AOPs because we count every single depth as a single data point. The three datasets with the largest amount of data (where each station, depth and variable count as a data point) were those provided by Ackleson, Mouw and Stramski/Reynolds. The Ackleson dataset contains data for seven IOPs and R_{rs}, Mouw provides data for nine IOPs as well as R_{rs} and the Stramski/Reynolds dataset has data
420 for six IOPs plus R_{rs}. Data from the largest datasets are also geographically diverse. Specifically, the Stramski/Reynolds dataset includes between 21 and 57 different geographic stations depending on the IOP data variable, the Mouw dataset includes between 63 and 102 different geographic stations and the Ackleson dataset provides between nine and 33 different geographic stations. Of note, from the BIOSOPE collaborative cruise, coincident BIOSOPE AOP and IOP data is provided by a suite of contributors. In this manuscript, BIOSOPE data
425 contributors and variables include Bricaud (a_{cdom}, a_{nap}, a_p), Lewis (R_{rs}) and Stramski/Reynolds (b_b).

11

Similar to the synergies of the BIOSOPE campaign with multiple investigators, dataset users are also encouraged to consider harnessing provided data to derive additional desired variables. For example, many stations contain a complete set of both an AOP measurement (R or R_{rs}) and the two main IOPs (a and b_b). Note that total absorption can

435 be calculated if all constituent absorption coefficients are measured in conjunction with published IOPs of pure water; this applies to most of our stations. Derivation and combinations of provided data ultimately depend on the intent and goals of the user.

We show the range in reflectance values (R_{rs}) provided from diverse geographic locations of inland, estuary, coastal,

440 open ocean and polar waters in Fig. 4. The diversity in the signal from inland water (Fig. 4, f) to coastal (Fig. 4, a, d, g), Arctic (Fig. 4, b) and open ocean waters (Fig. 4, c, e, h) show a range of the various particulate, biogeochemical, and other water conditions characteristic of different aquatic environments. The graphs also show the level of detail that can be extracted by varying spectral resolutions. Lower spectral resolution is shown in the Boss/Chase Arctic data (from 5 nm to tens of nm separation), and higher resolution is found in Boss/Chase Tara Oceans, Lewis and Mouw

445 (2–3 nm spectral resolution) and Ackleson, Craig, Schaeffer, and Stramski/Reynolds (1 nm spectral resolution).

When assessing the geographic distribution of the coincident IOP and AOP data, we found data were more frequent for latitudes between 30°N and 40°N and longitudes between 50°W and 100°W (Fig. 5). The Ackleson (San Francisco Bay), Schaeffer (northern Gulf of Mexico) and Mouw (Lake Superior) data were acquired at those latitudes and

450 longitudes. These results also highlight the lack of data for the area between 100°E and 180°E and at latitudes south of 50°.

We caution users of the datasets to consider inherent limitations to certain data collections. For example, some data collected in turbid waters were found to contain less signal compared to noise. Specifically, the AC-S dataset of

455 Boss/Chase has significant uncertainties in a_p in the blue part of the spectrum due to uncertainty in the scattering correction of this measurement, particularly in turbid waters (e.g. Stockley et al., 2017). Additionally, as previously detailed, not all data collected is coincident. We have indicated in Fig. 3 and Table 3 and several details including the geographic and variable distribution concerning coincident data. Overall, because most data have already been published in peer review literature with study collection, processing and analysis details and where needed fully

460 detailed here; readers are able to determine the utility and applicability of the datasets provided toward further use of the data.

5 Summary

We have compiled aquatic data from a variety of inland, coastal, estuary, and open ocean equatorial, mid- and high-

465 latitude locations. This compilation of aquatic data is a first step in achieving a global distribution of high spectral resolution IOP and AOP data, which we encourage the community to use for aquatic remote sensing algorithm

development and related activities. We recommend further in situ campaigns be commissioned to collect coincident high spectral resolution IOP and AOP data over regions with limited current coverage, for example, high latitude, inland and southerly waters. Such data could also be collected via and in conjunction with upcoming airborne high spectral resolution remote sensing campaigns. Additional in situ data collection over gap areas would be helpful in development, calibration and validation of global algorithms.

As additional high spectral resolution IOP/AOP data become available, this dataset can be expanded accordingly. A comprehensive collection of hyperspectral IOP/AOP datasets would be extremely useful for both development of aquatic remote sensing algorithms, and for the planning of future field sampling missions to address identified gaps. Future expansion of this collection of datasets, beyond addition of optical data, could be inclusion of biogeochemical information (e.g. phytoplankton pigments, carbon stocks, turbidity, particulate size distribution, and phytoplankton composition) to further assist in development of algorithms relating to biogeochemical parameters. It is crucial to collect coincident high spectral resolution IOP and AOP remote sensing data for the development of robust algorithms. These data, algorithms and scientific investigations can improve our understanding of Earth system biogeochemical, ecological and physical processes on local to global scales.

Author Contribution

The initial concept for this effort came from the NASA PACE Mission early science project discussions on a goal to provide the community with high spectral resolution datasets. CR and EB sent initial community requests for in situ aquatic data contributions. KC gathered and stewarded the data organization effort. KC led preparation, writing of the manuscript and generation of figures and tables. All data providers assisted in writing the methods of their data collection. All co-authors contributed to the scientific discussion, review and editing of the manuscript.

Competing interests

The authors declare that they have no conflicts of interest.

References

520   Allali, K., Bricaud, A., and Claustre, H.: Spatial variations in the chlorophyll-specific absorption coefficients of phytoplankton and photosynthetically active pigments in the equatorial Pacific, J Geophys Res, 102, C6, 12,413-12,423, doi:10.1029/97JC00380, 1997.

Astuti, I.S., Mishra, D.R., Mishra, S. and Schaeffer, B.: Spatio-temporal dynamics of inherent optical properties in

525   oligotrophic northern Gulf of Mexico estuaries, Cont Shelf Res, 166, 92-107, doi:10.1016/j.csr.2018.06.016, 2018.

Bell, T.W., Cavanaugh, K.C., and Siegel, D.A.: Remote monitoring of giant kelp biomass and physiological condition: An evaluation of the potential for the Hyperspectral Infrared Imager (HyspIRI) mission, Remote Sens Environ, 167, 218-228, doi:10.1016/j.rse.2015.05.003, 2015.

530

Bricaud, A., and Stramski, D.: Spectral absorption coefficients of living phytoplankton and nonalgal biogenous matter: A comparison between the Peru upwelling area and the Sargasso Sea, Limnol Oceanogr, 35, 3, 562-582, doi:10.4319/lo.1990.35.3.0562, 1990.

535   Bricaud, A., Babin, M., Claustre, H., Ras, J. and Tièche, F.: Light absorption properties and absorption budget of Southeast Pacific waters, J Geophys Res, 115, C08009, doi:10.1029/2009JC005517, 2010.

Boss, E., Picheral, M., Leeuw, T., Chase, A., Karsenti, E., Gorsky, G., Taylor, L., Slade, W., Ras, J., and Claustre, H.: The characteristics of particulate absorption, scattering and attenuation coefficients in the surface ocean; Contribution
540   of the Tara Oceans expedition, Methods Oceanogr, 7, 52-62, doi:10.1016/j.mio.2013.11.002, 2013.

Carder, K.L., and Steward, R.G.: A remote-sensing reflectance model of a red-tide dinoflagellate off west Florida, Limnol Oceanogr, 30, 2, 286-298, 1985.

545   Casey, K.A., Rousseaux, C.S., Gregg, W.W., Boss, E., Chase, A.P., Craig, S.E., Mouw, C.B., Reynolds, R.A., Stramski, D., Ackleson, S.G., Bricaud, A., Schaeffer, B., Lewis, M.R., and Maritorena, S.: In situ high spectral resolution inherent and apparent optical property data from diverse aquatic environments, PANGAEA, https://doi.pangaea.de/10.1594/PANGAEA.902230, 2019.

550   Chase, A.P., Boss, E., Cetinić, I., and Slade, W.: Estimation of phytoplankton accessory pigments from hyperspectral reflectance spectra: toward a global algorithm, J Geophys Res-Oceans, 122, 12, 9725-9743, doi:10.1002/2017JC012859, 2017.

Claustre, H., Sciandra, A., and Vaulot, D.: Introduction to the special section Bio-optical and biogeochemical
555   conditions in the South East Pacific in late 2004: the BIOSOPE program. Biogeosciences, 5, 679-691, 2008.

Conmy, R.N., Schaeffer, B.A., Schubauer-Berigan, J., Aukamp, J., Duffy, A., Lehrter, J.C., and Greene, R.M.: Characterizing light attenuation within northwest Florida estuaries: Implications for RESTORE Act water quality monitoring, Mar Pollut Bull, 114, 995-1006, doi:10.1016/j.marpolbul.2016.11.030, 2017.
560

Corson, M.R., and Davis, C.O.: A new view of coastal oceans from the space station, Eos, 92, 19, 161-162, doi:10.1029/2011EO190001, 2011.

Craig, S. E.: Spectral measurements of absorption, scattering and in vivofluorescence from phytoplankton cultures,
565   Department of Physics and Applied Physics, pp. 228, Glasgow: University of Strathclyde, 1999.

Craig, S.E., Jones, C.T., Li, W.K.W., Lazin, G., Horne, E., Caverhill, C., and Cullen, J.J.: Deriving optical metrics of coastal phytoplankton biomass from ocean colour, Remote Sens Environ, 119, 72-83, doi:10.1016/j.rse.2011.12.007, 2012.
570

Dall'Olmo, G., Westberry, T.K., Behrenfeld, M.J., Boss, E., and Slade, W.H.: Significant contribution of large particles to optical backscattering in the open ocean, Biogeosciences, 6, 947-967, 2009.

Del Castillo, C.E., Signorini, S.R., Karaköylü, and Rivero-Calle, S.: Is the Southern Ocean Getting Greener?, Geophys

575   Res Lett, 46, doi:10.1029/2019GL083163, 2019.

Devred, E., Turpie, K.R., Moses, W., Klemas, V.V., Moisan, T., Babin, M., Toro-Farmer, G., Forget, M.-H., and Jo, Y.-H.: Future retrievals of water column bio-optical properties using the Hyperspectral Infrared Imager (HyspIRI), Remote Sens-Basel, 5, 12, 6812-6837, doi:10.3390/rs5126812, 2013.

580
Dierssen, H.M., Chlus, A., and Russell, B.: Hyperspectral discrimination of floating mats of seagrass wrack and the macroalgae Sargassum in coastal waters of Greater Florida Bay using airborne remote sensing, Remote Sens Environ, 167, 247-258, doi:10.1016/j.rse.2015.01.027, 2015.

585   Dutkiewicz, S., Hickman, A.E., Jahn, O., Henson, S., Beaulieu, C., and Monier, E.: Ocean colour signature of climate change, Nat Commun, 10, 578, doi:10.1038/s41467-019-08457-x, 2019.

Freeman, L.A., Ackleson, S.G., and Rhea, W.J.: Comparison of remote sensing algorithms for retrieval of suspended particulate matter concentration from reflectance in coastal waters, J Appl Remote Sens, 11, 4, 046028,

590   doi:10.1117/1.JRS.11.046028, 2017.

Gould, R.W., Jr., Arnone, R.A. and Martinolich, P.M.: Spectral dependence of the scattering coefficient in case 1 and case 2 waters, Appl Optics, 38, 12, 2377-2383, 1999.

595   Gould, R.W., Jr., Arnone, R.A. and Sydor, M.: Absorption, scattering, and remote-sensing reflectance relationships in coastal waters: Testing a new inversion algorithm, J Coastal Res, 17, 2, 328-341, 2001.

Gordon, H.R., Lewis, M.R., McLean, S.D., Twardowski, M.S., Freeman, S.A., Voss, K.J., and Boynton, G.C.: Spectra of particulate backscattering in natural waters, Opt Express, 17, 18, 16192-16208, 2009.

600
Hu, C., Feng, L., Hardy, R.F., and Hochberg, E.J.: Spectral and spatial requirements of remote sensing measurements of pelagic Sargassum macroalgae, Remote Sens Environ, 167, 229-246, doi:10.1016/j.rse.2015.05.022, 2015.

Hu, C., Lee, Z., and Franz, B.: Chlorophyll *a* algorithms for oligotrophic oceans: A novel approach based on three-

605   band reflectance difference, J Geophys Res, 117, C01011, doi:10.1029/2011JC007395, 2012.

Keith, D.J., Schaeffer, B.A., Lunetta, R.S., Gould, R.W., Rocha, K., and Cobb, D.J.: Remote sensing of selected water-

quality indicators with the hyperspectral imager for the coastal ocean (HICO) sensor, Int J Remote Sens, 35, 9, 2927-2962, doi:10.1080/01431161.2014.894663, 2014.

610

Keith, D.J., Lunetta, R.S., and Schaeffer, B.A.: Optical models for remote sensing of colored dissolved organic matter absorption and salinity in New England, Middle Atlantic and Gulf Coast Estuaries USA, Remote Sens-Basel, 8, 283, doi:10.3390/rs8040283, 2016.

615 Kim, G.E., Gnanadesikan, A., Del Castillo, C.E., Pradal, M.-A.: Upper ocean cooling in a coupled climate model due to light attenuation by yellowing materials, Geophys Res Lett, 45, 6134-6140, doi:10.1029/2018GL077297, 2018.

Kishino, M., Takahashi, M. Okami, N. Ichimura, S.: Estimation of the spectral absorption coefficients of phytoplankton in the sea, B Mar Sci, 37, 2, 634-642, 1985.

620

Le, C., Lehrter, J.C., Hu, C., Schaeffer, B.A., MacIntyre, H., Hagy, J.D., Beddick, D.L.: Relation between inherent optical properties and land use and land cover across Gulf Coast estuaries, Limnol Oceanogr, 60, 3, 920-933, doi:10.1002/lno.10065, 2015.

625 Le, C., Lehrter, J.C., Schaeffer, B.A., Hu, C., Murrell, M.C., Hagy, J.D., Greene, R.M., and Beck, M.: Bio-optical water quality dynamics observed from MERIS in Pensacola Bay, Florida, Estuar Coast Shelf S, 173, 26-38, doi:10.1016/j.ecss.2016.02.003, 2016.

Lee, Z., Shang, S., Hu, C., Lewis, M., Arnone, R., Li, Y., and Lubac, B.: Time series of bio-optical properties in a 630 subtropical gyre: Implications for the evaluation of interannual trends of biogeochemical properties, J Geophys Res-Oceans, 115(C9), 2010.

Lin, J., Lee, Z., Ondrusek, M., and Liu, X.: Hyperspectral absorption and backscattering coefficients of bulk water retrieved from a combination of remote-sensing reflectance and attenuation coefficient, Opt Express, 26, 2, A157-635 A177, doi:10.1364/OE.26.00A157, 2018.

Lohrenz, S.E.: A novel theoretical approach to correct for pathlength amplification and variable sampling loading in measurements of particulate spectral absorption by the quantitative filter technique, J Plankton Res, 22, 4, 639-657, doi:10.1093/plankt/22.4.639, 2000.

640

Lohrenz, S.E., Weidemann, A.D. and Tuel, M.: Phytoplankton spectral absorption as influenced by community size structure and pigment composition, J Plankton Res, 25, 1, 35-61, doi:10.1093/plankt/25.1.35, 2003.

17

Loisel, H., Stramski, D., Dessaily, D., Jamet, C., Li, L., Reynolds, R.A.: An inverse model for estimating the optical

645 absorption and backscattering coefficients of seawater from remote-sensing reflectance over a broad range of oceanic

and coastal marine environments, J Geophys Res-Oceans, 123, 2141-2171, doi:10.1002/2017JC013632, 2018.

Matsuoka, A., Boss, E., Babin, M., Karp-Boss, L., Hafez, M., Chekalyuk, A., Proctor, C.W., Werdell, P.J., and

Bricaud, A.: Pan-Arctic optical characteristics of colored dissolved organic matter: Tracing dissolved organic carbon

650 in changing Arctic waters using satellite ocean color data, Remote Sens Environ, 200, 89-101, 2017.

McClain, C.R.: A decade of satellite ocean color observations, Annu Rev Mar Sci, 1, 19-42,

doi:10.1146/annurev.marine.010908.163650, 2009.

655 Mishra, D., Schaeffer, B.A. and Keith, D.: Performance evaluation of normalized difference chlorophyll index in

northern Gulf of Mexico estuaries using the Hyperspectral Imager for the Coastal Ocean, GISci Remote Sens, 51, 2,

175-198, doi:10.1080/15481603.2014.895581, 2014.

Mobley, C.D.: Estimation of the remote-sensing reflectance from above-surface measurements, Appl Optics, 38, 36,

660 7442-7455, doi:10.1364/AO.38.007442, 1999.

Mobley, C.D., and Stramski, D.: Origins of variability in remote-sensing reflectance. Final Report. Sequoia Scientific,

Redmond, WA, 1997.

665 Mouw, C.B., Greb, S., Aurin, D., DiGiacomo, P.M., Lee, Z., Twardowski, M., Binding, C., Hu, C., Ma, R., Moore,

T., Moses, W. and Craig, S.E.: Aquatic color radiometry remote sensing of coastal and inland waters: Challenges and

recommendations for future satellite missions, Remote Sens Environ, 160, 15–30, doi:10.1016/j.rse.2015.02.001,

2015.

670 Mouw, C.B., Ciochetto, A., Grunert, B., and Yu, A.: Expanding understanding of optical variability in Lake Superior

with a 4-year dataset, Earth Syst Sci Data, 9, 497-509, doi:10.5194/essd-9-497-2017, 2017.

Mueller, J.L., Morel, A., Frouin, R., Davis, C., Arnone, R., Carder, K., Lee, Z.P., Steward, R.G., Hooker, S.B.,

Mobley, C.D., McLean, S., Holben, B., Miller, M., Pietras, C., Knobelspiesse, K.D., Fargion, G.S., Porter, J., and

675 Voss, K.J.: Radiometric measurements and data analysis protocols. In J.L. Mueller, G.S. Fargion, & C.R. McClain

(Eds.), Ocean optics protocols for satellite ocean colour sensor validation, Revision 4, Volume IV, Greenbelt, MD:

NASA, Goddard Space Flight Center, NASA/TM-2003-211621, 84 pp., 2003.

NASA Goddard Space Flight Center, Ocean Ecology Laboratory, Ocean Biology Processing Group, Sea-viewing
680   Wide Field-of-view Sensor (SeaWiFS) Ocean Color Data, NASA OB.DAAC, doi: 10.5067/ORBVIEW-
2/SEAWIFS_OC.2014.0, 2014.

National Academies of Sciences, Engineering, and Medicine, Thriving on Our Changing Planet: A Decadal Strategy
for Earth Observation from Space, Washington, D.C., The National Academies Press. doi:10.17226/24938, 2018.
685

Neukermans, G., Reynolds, R.A., and Stramski, D.: Optical classification and characterization of marine particle
assemblages within the western Arctic Ocean, Limnol Oceanogr, 61, 1472-1494. doi: 10.1002/lno.10316, 2016.

O'Reilly, J.E., and Werdell, P.J.: Chlorophyll algorithms for ocean color sensors – OC4, OC5 & OC6, Remote Sens
690   Environ, 229, 32-47, doi:10.1016/j.rse.2019.04.021, 2019.

O'Reilly, J.E., Maritorena, S., Mitchell, B.G., Siegel, D.A., Carder, K.L. Garver, S.A., Kahru, M. and McClain, C.:
Ocean color chlorophyll algorithms for SeaWiFS, J Geophys Res, 103, C11, 24937-24953, doi:10.1029/98JC02160,
1998.
695

Pahlevan, N., Chittimalli, S.K., Balasubramanian, S.V., and Vellucci, V.: Sentinel-2/Landsat-8 product consistency
and implications for monitoring aquatic systems, Remote Sens Environ, 220, 19-29, doi:10.1016/j.rse.2018.10.027,
2019.

700   Pegau, S., Zaneveld, J.R.V., Mitchell, B.G., Mueller, J.L., Kahru, M., Wieland, J., and Stramska, M.: Inherent Optical
Properties: Instruments, Characterizations, Field Measurements and Data Analysis Protocols. In J.L. Mueller, G.S.
Fargion, & C.R. McClain (Eds.), *Ocean optics protocols for satellite ocean colour sensor validation, Revision 4,
Volume IV,* Greenbelt, MD: NASA, Goddard Space Flight Center, NASA/TM-2003-211621, 84 pp, 2003.

705   Röttgers, R., and Doerffer, R.: Measurements of optical absorption by chromophoric dissolved organic matter using
a point-source integrating cavity absorption meter, Limnol Oceanogr-Meth, 5, 126-135, 2007.

Schaeffer, B.A., Conmy, R.N., Duffy, A., Aukamp, J., Yates, D., and Craven, G., Northern Gulf of Mexico estuarine
colored dissolved organic matter derived from MODIS data, Int J Remote Sens, 36:8, 2219-2237, 2015.
710

Shibata, K.: Spectrophotometry of translucent biological materials - opal glass transmission method, In D. Glick (Ed.),
Methods of Biochemical Analysis. New York: Interscience Publishers Inc., 1959.

19

Slade, W.H., Boss, E., Dall'olmo, G., Langner, M.R., Loftin, J., Behrenfeld, M.J., Roesler, C., and Westberry, T.K.: Underway and moored methods for improving accuracy in measurement of spectral particulate absorption and attenuation, J Atmos Ocean Tech, 27, 1733-1746, doi:10.1175/2010JTECHO755.1, 2010.

Stockley, N.D., Röttgers, R., McKee, D., Lefering, I., Sullivan, J.M., and Twardowski, M.S.: Assessing uncertainties in scattering correction algorithms for reflective tube absorption measurements made with a WET Labs ac-9, Opt Express, 25, 24, A1139-A1153, doi:10.1364/OE.25.0A1139, 2017.

Stramski, D., Reynolds, R.A., Babin, M., Kaczmarek, S., Lewis, M.R., Röttgers, R., Sciandra, A., Stramska, M., Twardowski, M.S., Franz, B.A., and Claustre, H.: Relationships between the surface concentration of particulate organic carbon and optical properties in the eastern South Pacific and eastern Atlantic Oceans, Biogeosciences, European Geosciences Union, 5, 1, 171-201, 2008.

Stramski, D., Reynolds, R.A., Kaczmarek, S., Uitz, J., Zheng, G.: Correction of pathlength amplification in the filter-pad technique for measurements of particulate absorption coefficient in the visible spectral region, Appl Optics, 54, 22, 6763-6782, doi:10.1364/AO.54.006763, 2015.

Tassan, S., and Ferrari, G.M.: An alternative approach to absorption measurements of aquatic particles retained on filters, Limnol Oceanogr, 40, 8, 1358-1368, 1995.

Torrecilla, E., Stramski, D., Reynolds, R.A., Millan-Núñez, E., and Pierra, J.: Cluster analysis of hyperspectral optical data for discriminating phytoplankton pigment assemblages in the open ocean, Remote Sens Environ, 115, 2578-2593, doi:10.1016/j.rse.2011.05.014, 2011.

Uitz, J., Stramski, D., Reynolds, R.A., and Dubranna, J.: Assessing phytoplankton community composition from hyperspectral measurements of phytoplankton absorption coefficient and remote-sensing reflectance in open-ocean environments, Remote Sens Environ, 171, 58-74, doi:10.1016/j.rse.2015.09.027, 2015.

Valente, A., Sathyendranath, S., Brotas, V., Groom, S., Grant, M., Taberner, M., Antoine, D., Arnone, R., Balch, W.M., Barker, K., Barlow, R., Bélanger, S., Berthon, J.-F., Besiktepe, S., Borsheim, Y., Bracher, A. ,Brando, V., Canuti, E., Chavez, F., Cianca, A., Claustre, H., Clementson, L., Crout, R., Frouin, R., García-Soto, C., Gibb, S.W., Gould, R., Hooker, S.B., Kahru, M., Kampel, M., Klein, H., Kratzer, S., Kudela, R., Ledesma, J., Loisel, H., Matrai, P., McKee, D., Mitchell, B.G., Moisan, T., Muller-Karger, F., O'Dowd, L., Ondrusek, M., Platt, T., Poulton, A.J., Repecaud, M., Schroeder, T., Smyth, T., Smythe-Wright, D., Sosik, H.M., Twardowski, M., Vellucci, V., Voss, K., Werdell, J., Wernand, M., Wright, S., and Zibordi, G.: A compilation of global bio-optical in situ data for ocean-colour satellite applications – version two, Earth Syst Sci Data, 11, 1037-1068, doi:10.5194/essd-11-1037-2019, 2019.

20

Vandermeulen, R.A., Mannino, A., Neeley, A., Werdell, J. and Arnone, R.: Determining the optimal spectral sampling frequency and uncertainty thresholds for hyperspectral remote sensing of ocean color, Opt Express, 25, 16, A785–13, doi:10.1364/OE.25.00A785, 2017.

755   Wang, G., Lee, Z., Mishra, D.R., and Ma, R.: Retrieving absorption coefficients of multiple phytoplankton pigments from hyperspectral remote sensing reflectance measured over cyanobacteria bloom waters, Limnol Oceanogr-Meth, 14, 7, 432–447, doi:10.1002/lom3.10102, 2016.

Werdell, P.J., and Bailey, S.W.: The SeaWiFS Bio-optical Archive and Storage System (SeaBASS): Current
760   architecture and implementation, NASA Tech. Memo. 2002-211617 , G.S. Fargion and C.R. McClain, Eds., NASA Goddard Space Flight Center, Greenbelt, Maryland, 45 pp, 2002.

Werdell, P.J., and Bailey, S.W.: An improved in-situ bio-optical data set for ocean color algorithm development and satellite data product validation, Remote Sens Environ, 98, 122-140, doi:10.1016/j.rse.2005.07.001, 2005.

765

Werdell, P.J., McKinna, L.I.W., Boss, E., Ackleson, S.G., Craig, S.E., Gregg, W.W., Lee, Z., Maritorena, S., Roesler, C.S., Rousseaux, C.S., Stramski, D., Sullivan, J.M., Twardowski, M.S., Tzortziou, M., and Zhang, X.: Prog Oceanogr, 160, 186-212, doi:10.1016/j.pocean.2018.01.001, 2018.

770   Werdell, P.J., Behrenfeld, M.J., Bontempi, P.S., Boss, E., Cairns, B., Davis, G.T., Franz, B.A., Gliese, U.B., Gorman, E.T., Hasekamp, O., Knobelspiesse, K.D., Mannino, A., Martins, J.V., McClain, C.R., Meister, G., and Remer, L.A.: The Plankton, Aerosol, Cloud, Ocean Ecosystem Mission: Status, Science, Advances, B Am Meteorol Soc, 100, 1775–1794, https://doi.org/10.1175/BAMS-D-18-0056.1, 2019.

775   Zheng, G., Stramski, D., and Reynolds, R.A.: Evaluation of the Quasi-Analytical Algorithm for estimating the inherent optical properties of seawater from ocean color: Comparison of Arctic and lower-latitude waters, Remote Sens Environ, 155, 194-209, doi:10.1016/j.rse.2014.08.020, 2014.

780

Variable	Definition, Units
$a(\lambda)$	Total absorption equal to sum of particulate absorption, CDOM absorption and water absorption (m^{-1})
$a_{cdom}(\lambda)$	Colored dissolved organic matter (CDOM) absorption coefficient (m^{-1})
$a_{cdom\_dis}(\lambda)$	Discrete CDOM absorption coefficient (m^{-1})
$a_{cdom\_int}(\lambda)$	Interpolated CDOM absorption coefficient (m^{-1})
$a_{cdom\_unc}(\lambda)$	Uncertainty in measured CDOM absorption coefficient (m^{-1})

$a_{nap}(\lambda)$	Non-algal particle absorption coefficient (m^{-1})
$a_{nap\_dis}(\lambda)$	Discrete non-algal particle absorption coefficient (m^{-1})
$a_{nw}(\lambda)$	Measured absorption with pure water subtracted (m^{-1})
$a_{p}(\lambda)$	Particulate absorption coefficient (m^{-1})
$a_{p\_dis}(\lambda)$	Discrete particulate absorption coefficient (m^{-1})
$a_{p\_unc}(\lambda)$	Uncertainty in particulate absorption coefficient (m^{-1})
$a_{ph}(\lambda)$	Phytoplankton absorption coefficient (m^{-1})
$b_{b}(\lambda)$	Total backscattering coefficient (m^{-1})
$b_{bp}(\lambda)$	Particulate backscattering coefficient (m^{-1})
$c(\lambda)$	Total attenuation equal to sum of particulate attenuation, CDOM attenuation and water attenuation (m^{-1})
$c_{nw}(\lambda)$	Measured attenuation with pure water subtracted (non-water attenuation) (m^{-1})
$c_{p}(\lambda)$	Particulate attenuation coefficient (m^{-1})
$c_{p\_unc}(\lambda)$	Uncertainty in particulate attenuation coefficient (m^{-1})
$R(\lambda)$	Irradiance reflectance (dimensionless)
$R_{stdv}(\lambda)$	Standard deviation of irradiance reflectance (dimensionless)
$R_{rs}(\lambda)$	Remote-sensing reflectance (sr^{-1})
$R_{rs\_stdv}(\lambda)$	Standard deviation of remote-sensing reflectance (sr^{-1})

795 **Table 1. List of variables included in the database. Variables are provided as defined by contributor. The symbol 'λ' represents light wavelength in vacuum, in units of nanometer (nm). The term 'discrete' is used to indicate a water sample removed from the aquatic environment.**

800

Contributor	Cruise	Location	Collection dates	Parameters measured / derived	Collection instrument(s)	Publications
Ackleson	RIO-SFE-1 RIO-SFE-3	San Francisco Bay	5/2014; 3/2015	$a(\lambda)$, $a_{cdom}(\lambda)$, $a_{cdom\_int}(\lambda)$, $a_{nw}(\lambda)$, $b_{b}(\lambda)$, $c(\lambda)$, $c_{nw}(\lambda)$, $R_{rs}(\lambda)$, $R_{rs\_stdv}(\lambda)$	WET Labs spectral ac meters (AC-S, AC-9); ASD Fieldspec HandHeld	Freeman et al., 2017
Boss, Chase	Tara Oceans /	Atlantic, Indian, Pacific, Mediterranean	1/2010– 3/2012;	$a_{p}(\lambda)$, $a_{p\_unc}(\lambda)$, $c_{p}(\lambda)$, $c_{p\_unc}(\lambda)$, $R_{rs}(\lambda)$, $R_{rs\_stdv}(\lambda)$	AC-S, HyperPro in buoy mode	Boss et al., 2013, Chase et al., 2017

Deleted: ¶

22

	Tara Med / SABOR	Sea, coastal and open ocean waters	6/2014– 9/2014			
Boss, Chase	Tara Arctic	Arctic coastal and open ocean waters	5/2013– 10/2013	$a_{cdom}(\lambda)$, $a_{cdom\_unc}(\lambda)$, $a_p(\lambda)$, $a_{p\_unc}(\lambda)$, $c_p(\lambda)$, $c_{p\_unc}(\lambda)$, $R_{rs}(\lambda)$, $R_{rs\_stdv}(\lambda)$	AC-S, C-OPS profiling radiometer	Chase et al., 2017; Matsuoka et al., 2017
Bricaud	BIOSOPE	Southeast Pacific ocean	10/2004– 12/2004	$a_{cdom}(\lambda)$, $a_{nap}(\lambda)$, $a_p(\lambda)$	WPI Ultrapath; Perkin-Elmer Lambda 19 spectrophotometer with integrating sphere	Claustre, et al., 2008; Bricaud et al., 2010
Craig	BBOMB	Coastal Northwest Atlantic ocean	2/2009– 3/2010	$a_{nap}(\lambda)$, $a_p(\lambda)$, $a_{ph}(\lambda)$, $R_{rs}(\lambda)$	HyperPro, Cary 4000 UV-vis spectrophotometer	Craig et al., 2012
Lewis	BIOSOPE	Southeast Pacific ocean	1/2004– 12/2004	$R(\lambda)$, $R_{stdv}(\lambda)$, $R_{rs}(\lambda)$, $R_{rs\_stdv}(\lambda)$	HyperPro in buoy mode	Claustre, et al., 2008; Stramski et al., 2008; Lee et al., 2010
Mouw	Several studies in Lake Superior	Lake Superior, USA	6/2013– 5/2016	$a(\lambda)$, $a_{cdom}(\lambda)$, $a_{cdom\_dis}(\lambda)$, $a_{nap\_dis}(\lambda)$, $a_{nw}(\lambda)$, $a_p(\lambda)$, $a_{p\_dis}(\lambda)$, $b_b(\lambda)$, $b_{bp}(\lambda)$, $c(\lambda)$, $c_{nw}(\lambda)$, $R_{rs}(\lambda)$	HyperOCR spectral radiometers, WET Labs AC-S, WET Labs ECO-BB9, WET Labs ECO-FL3, SeaBird CTD 37SI, Perkin Elmer Lambda 35	Mouw et al., 2017
Schaeffer	Florida Estuary Optics	Northern Gulf of Mexico estuaries, USA	9/2009– 11/2011	$a_{cdom}(\lambda)$, $a_{nap}(\lambda)$, $a_p(\lambda)$, $a_{ph}(\lambda)$, $R_{rs}(\lambda)$	HyperSAS, HyperPRO in profiling mode, Shimadzu UV1700	Astuti et al., 2018; Conmy et al., 2017; Keith et al., 2014; Keith et al., 2016; Le et al., 2015; Le et al., 2016; Mishra et al., 2014; Schaeffer et al., 2015

Deleted: South East

Deleted: Ocean

Deleted: South East

Deleted: Ocean

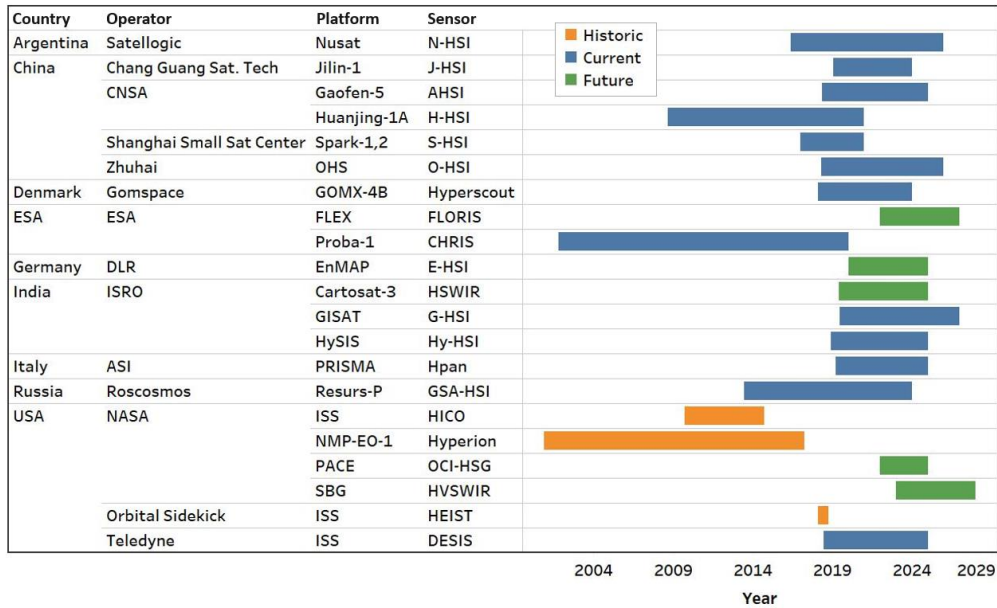| Stramski, Reynolds | BIOSOPE, ANT26, KM12 | Southeast and Tropical Pacific and Atlantic ocean | 10/2004–12/2004; 4/2010–5/2010; 6/2012 | $a_{cdom}(\lambda)$, $a_{nap}(\lambda)$, $a_p(\lambda)$, $a_{ph}(\lambda)$, $b_b(\lambda)$, $b_{bp}(\lambda)$, $R_{rs}(\lambda)$ | Perkin-Elmer Lambda 18 spectrophotometer with integrating sphere; HOBI Labs HS-6 or a-βeta; Satlantic HyperPro II in buoy mode | Stramski et al., 2008; Uitz et al., 2015; Loisel et al., 2018 |

Deleted: South East Pacific Ocean, Atlantic Ocean,

Deleted: Ocean

810 **Table 2. In situ data collection instrument, logistical details and related references.**

Deleted: ¶

	a	a_{cdom}	a_{cdom_dis}	a_{cdom_int}	a_{cdom_unc}	a_{nap}	a_{nap_dis}	a_{nw}	a_p	a_{p_dis}	a_{p_unc}	a_{ph}	b_b	b_{bp}	c	c_{nw}	c_p	c_{p_unc}	R	R_{stdv}	R_{rs}	R_{rs_stdv}
RIO-SFE-1,-3	22671 (9)	8831 (34)		22671 (9)				22671 (9)				22671 (9)			22671 (9)	22671 (9)					9 (9)	9 (9)
Tara Arctic		29 (29)			29 (29)				29 (9)		29 (9)						29 (9)	29 (9)			29 (9)	29 (9)
Tara Oceans/Med, SABOR									103 (101)		103 (101)						103 (101)	103 (101)			103 (101)	103 (101)
BIOSOPE (Bricaud)		109 (30)			138 (36)				141 (38)													
BBOMB								43 (1)	43 (1)			43 (1)									43 (1)	
BIOSOPE (Lewis)																			67 (66)	67 (66)	67 (66)	67 (66)
Lake Superior	2918 (84)	2597 (63)	183 (95)			209 (102)	2918 (84)		2462 (62)	204 (101)			2959 (84)	2959 (84)	2922 (84)	2918 (84)					80 (78)	
Florida Estuary Optics		719 (125)			719 (125)				718 (125)			719 (125)									621 (141)	
BIOSOPE (Stramski, Reynolds), ANT26, KM12		16 (16)			21 (21)				21 (21)			21 (21)	57 (57)	57 (57)							21 (21)	

Table 3: Data provided by each investigator and cruise. The number in the cells indicates the number of data points
815 **available. The number between parentheses is the number of stations in the dataset.**

Country	Operator	Platform	Sensor
Argentina	Satellogic	Nusat	N-HSI
China	Chang Guang Sat. Tech	Jilin-1	J-HSI
	CNSA	Gaofen-5	AHSI
		Huanjing-1A	H-HSI
	Shanghai Small Sat Center	Spark-1,2	S-HSI
	Zhuhai	OHS	O-HSI
Denmark	Gomspace	GOMX-4B	Hyperscout
ESA	ESA	FLEX	FLORIS
		Proba-1	CHRIS
Germany	DLR	EnMAP	E-HSI
India	ISRO	Cartosat-3	HSWIR
		GISAT	G-HSI
		HySIS	Hy-HSI
Italy	ASI	PRISMA	Hpan
Russia	Roscosmos	Resurs-P	GSA-HSI
USA	NASA	ISS	HICO
		NMP-EO-1	Hyperion
		PACE	OCI-HSG
		SBG	HVSWIR
	Orbital Sidekick	ISS	HEIST
	Teledyne	ISS	DESIS

820

Figure 1: Illustration of the historical, existing and planned high spectral resolution satellite mission country or agency, operator or agency, platform, sensor name and operation timeline.

825

25
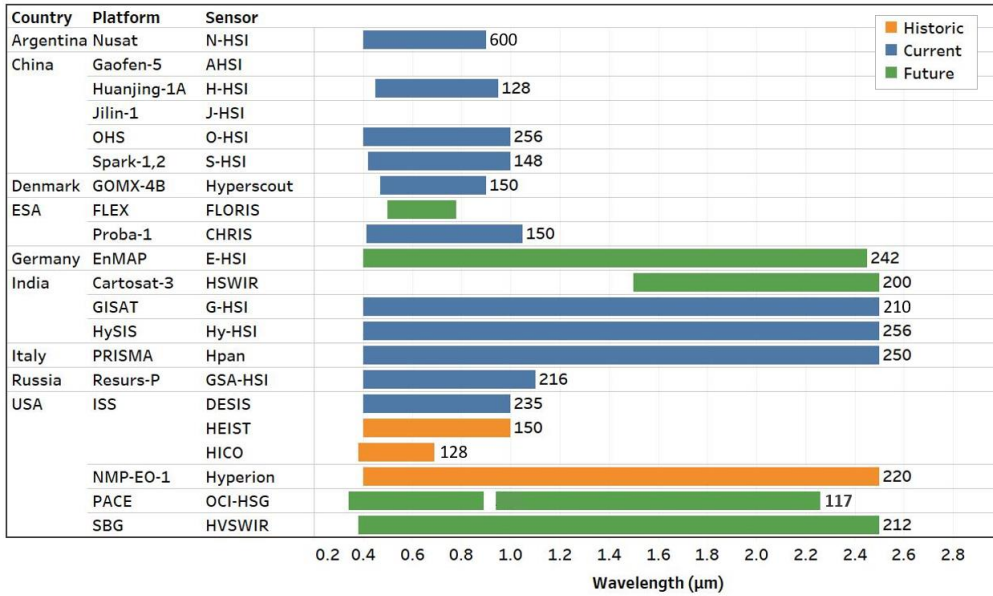
Figure 2: Listing of the spectral wavelength range and total number or sensor bands (right of each bar) where presently known for each of the high spectral resolution satellite missions.
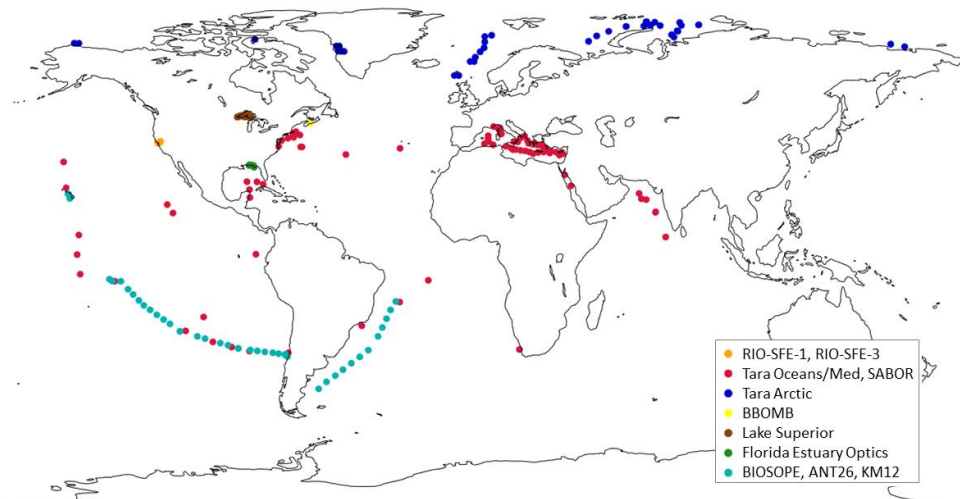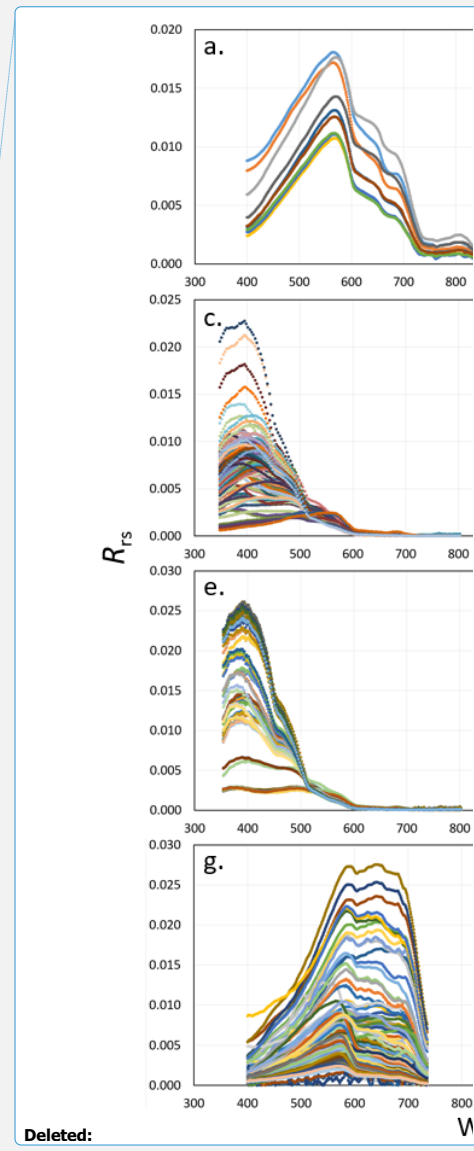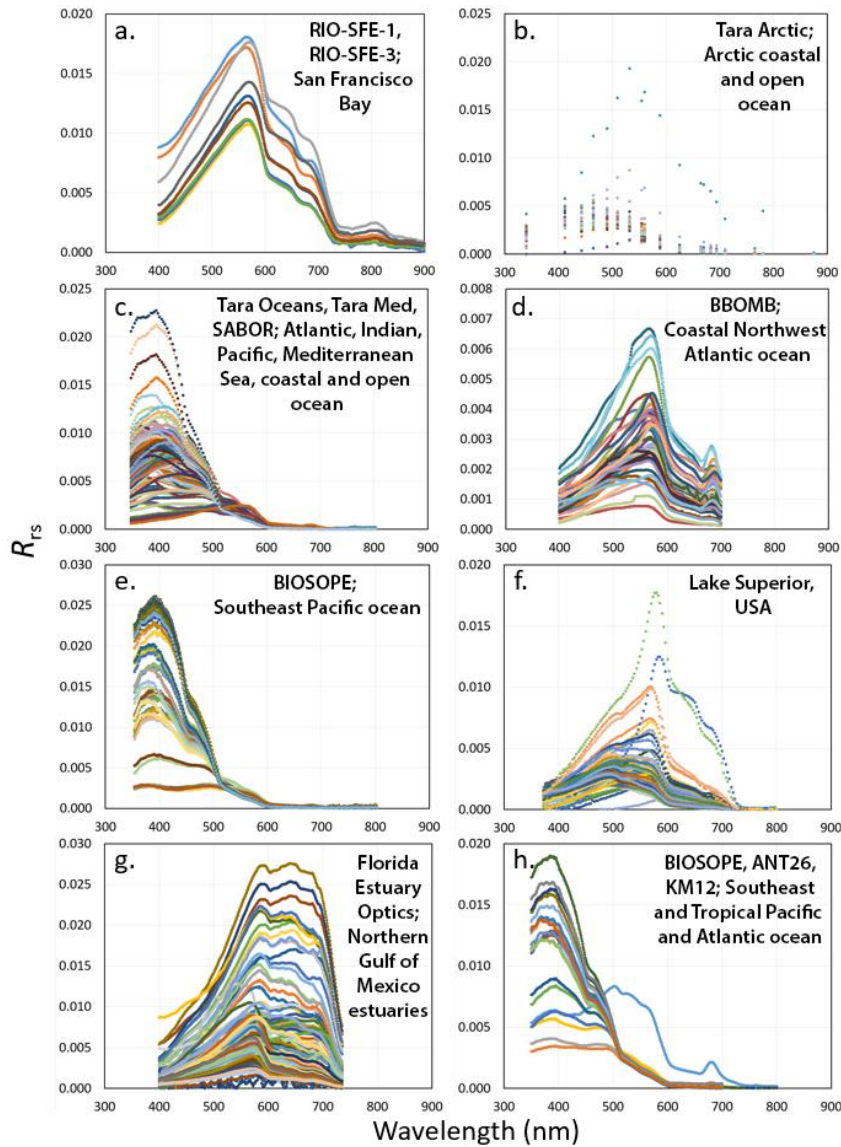
830

26

Coincident IOP/AOP

Figure 3: Global geographic distribution of coincident IOP/AOP data.

835

27

840 **Figure 4: Plots demonstrate spectral reflectance diversity of inland, estuary, and ocean environments (location information is provided in the Figure 3 global map). Reflectance distribution plots display R_{rs} data from (a.) San Francisco Bay waters (Ackleson), (b.) Arctic coastal and open ocean (Boss/Chase Arctic), (c.) Atlantic, Indian, Pacific, Mediterranean Sea, coastal and open ocean (Boss/Chase), (d.) coastal northwest Atlantic ocean (Craig), (e.) Southeast Pacific ocean (Lewis), (f.) Lake**

850   Superior, USA, inland water (Mouw), (g.) Northern Gulf of Mexico estuaries (Schaeffer) and (h.) Southeast and tropical Pacific and Atlantic ocean (Stramski/Reynolds). Note, subplots demonstrate the spectral sampling interval provided; where high spectral sampling interval data is available, subplots appear more 'linear' (a, d, g, h) and where there is lower spectral sampling interval data, subplots appear more 'point', less continuous (b, c, e, f). Each color in the subplot represents a separate data collection.
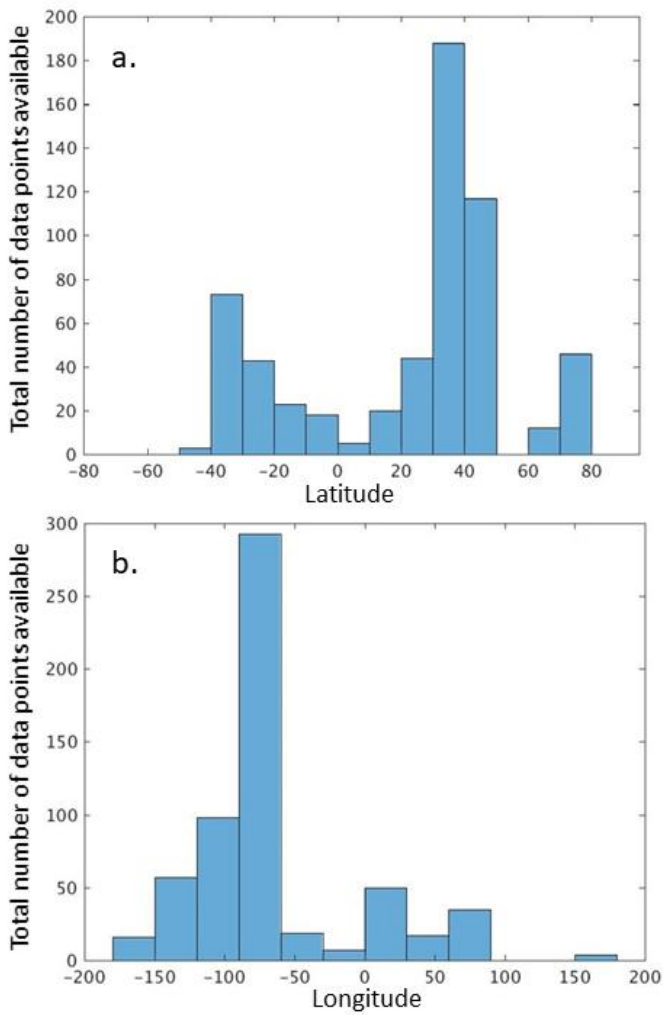
855

Figure 5: Geographic frequency distribution of stations with coincident IOP and AOP data. Plot (a) shows data point distribution by latitude and plot (b) shows data point distribution by longitude.